Properties of Poly(vinyl alcohol)—Bentonite Clay Nanocomposite Films in Relation to Polymer–Clay Interactions

A. A. Sapalidis, F. K. Katsaros, Th. A. Steriotis, N. K. Kanellopoulos

Institute of Physical Chemistry, NCSR Demokritos, Aghia Paraskevi Attikis 153 10 Athens, Greece

Received 10 November 2010; accepted 7 April 2011
DOI 10.1002/app.34651
Published online 22 August 2011 in Wiley Online Library (wileyonlinelibrary.com).

ABSTRACT: This study describes an effective way for the preparation of well-dispersed, high-loaded PVA/bentonite nanocomposites with improved properties, based on nanoscale interactions. To this end, a series of Poly(vinyl alcohol)—bentonite clay nanocomposites have been prepared via solvent casting technique and their properties were thoroughly investigated by atomic force microscopy, transmission electron microscopy, X-Ray diffraction, oxygen and water permeability, water sorption along with mechanical and thermal studies. Microscopic and XRD techniques revealed highly organized regions. Clay content up to 10% led to nanocomposites with high degree of exfoliation. In addition samples with increased filler content (20%) demonstrated also, apart from the delaminated, well-organized intercalated regions. The nanocomposites exhibited increased mechanical, thermal and gas barrier properties, though they retained their optical clarity. Thus, the Young's modulus of the sample containing 20% clay was increased by 193 times, while the oxygen permeability was decreased about seven times, in regard to the corresponding values of the neat polymer. The obtained results were explored on the basis of nanoscale phenomena and it was concluded that the organized structures and intercalated regions observed on highly loaded samples are attributed to the competitive effect between weaker polymer–polymer interactions in relation to stronger polymer–clay ones. © 2011 Wiley Periodicals, Inc. J Appl Polym Sci 123: 1812–1821, 2012

Key words: nanocomposites; barrier; diffusion; mechanical properties; clay

INTRODUCTION

Polymer nanocomposites represent a new class of material alternative to conventional filled polymers. In this new class of material, fillers (having at least one dimension in nanoscale) are dispersed in a polymer matrix offering remarkable improvement in performance properties of the polymer. Among all the potential nanocomposite fillers, those based on clay and layered silicates have been more widely investigated probably because the starting clay materials are easily available and because their intercalation chemistry has been studied for a long time.[1–3]

Since the properties are strongly related to nanoscale dispersion, these materials exhibit improved mechanical, thermal, optical and physicochemical properties, when compared with the pure polymer or conventional (microscale) composites.[4–9] Improvements may also include, for example, increased moduli, strength and heat resistance, decreased gas permeability and flammability.[3,10,11] The combination of enhanced properties and weight reduction has already led to several commercial applications. Nylon-layered silicate nanocomposites have already been applied in automotive industry by Toyota Motor Company, while nanocomposite barrier films are currently used for food packaging and other applications. Similar R&D efforts focusing on silicate nanocomposites are already underway worldwide. Potential applications include airplane interiors, fuel tanks, electrical or electronic components, under-the-hood structural parts, brakes, and tires.[12]

Poly(vinyl alcohol)—clay nanocomposite materials have been investigated in the past[13–16] and been synthesized by common solvent film casting method and *in situ* polymerization. Several types of clays have been used to produce these nanocomposite materials which include pristine clays and organoclays.[17] These materials have been tested for a variety of applications including wound dressing[18] and pervaporation membranes for dehydration.[19] More recently a highly ordered poly(vinyl alcohol)/montmorillonite nanocomposite produced by the layer by layer (LBL) process exhibited superior mechanical properties.[9]

The properties of PVA are strongly dependent on both intra and intermolecular interactions. On the other hand, bentonite clay particles carry two different kinds of electrical charges, the surface hydroxyl

Correspondence to: A. A. Sapalidis (asap@chem.demokritos.gr).

groups and the structural permanent negative sites, leading to their cation exchange capacity.[20] It is well known that certain metal ions can enter their crystal lattice,[21] affecting their surface charge and interlayer complexation ability.[22] In the case of nanocomposites, the formation of hydrogen bonds between the PVA's hydroxyl groups and the negatively charged clay surface, determine the effective dispersion of the inorganic layers. Thus, the addition of clay particles in a polymer solution causes the polymeric chains to adsorb on the solid's surface via complicated polymer–polymer and polymer–clay interactions.[23] These interactions enable the chains to receive certain conformations and to build structures around the inorganic layers. Depending on the nature of the adhesion (strong or weak) these arrangements lead to the formation of larger assemblies, like structured intercalated regions. Theoretical and experimental research results demonstrate that the adhesive role of a polar polymer between hydrophilic clay layers, the so called "glue effect," tends to strongly prohibit complete dissociation of the layered structure of the clay, resulting in only an ordered intercalated state.[24]

In previous studies, most authors, targeted to high matrix-clay interactions, used fully hydrolyzed PVA. The approach implemented in this study takes additionally into account the intramolecular interactions between polymer chains. The presence of acetoxy groups in the selected polymer (PVA, 88% hydrolysis grade) will lead to weaker polymer–polymer interactions. Additionally, the presence of metal cations in the clay lattice is expected to interact with the acetoxy groups of the PVA, as shown in previous studies,[21] promoting the synergetic effect between polymer chains and clay layers. To this end, a series of poly(vinyl alcohol)/bentonite clay composites were prepared using the common solvent film casting method. The nanocomposites exhibited high levels of clay organization inside the polymer matrix, due to favorable polymer–particle interactions, leading to unique properties. The produced materials were thoroughly characterized by wide angle X-ray diffraction (XRD), Scanning Electron Microscopy (SEM), Transmission Electron Microscopy (TEM), Atomic Force Microscopy (AFM), UV-Visible transmission spectroscopy, differential scanning calorimetry (DSC), thermogravimetric analysis (TGA), mechanical strength, oxygen and water permeability and water sorption studies.

EXPERIMENTAL

Materials and instrumentation

Low viscosity, partially hydrolyzed atactic poly(vinyl alcohol) Mowiol® 5–88 with a weight average molecular weight 37,000 g/mol was purchased by Sigma. Natural bentonite with cationic exchange capacity (CEC) value of 80 mequiv./100 g from the Milos island mine was kindly supplied by S and B Industrial Minerals S.A., Greece. Reverse osmosis (RO) water was used to prepare all aqueous solutions. XRD patterns were recorded on a Siemens XD-500 diffractometer using Cu Kα1 radiation with a scan rate of 0.03°/s. The patterns were collected using background-free holders. The optical spectra were collected on a Cary 100 Varian Inc. UV-Vis spectrophotometer. Surface morphology, was examined with a Digital Instruments Nanoscope III atomic force microscope (AFM). All AFM images were recorded in tapping mode. For the bentonite images, a clay solution of 100 mg L^{-1} was used to deposit the clay on a synthetic mica substrate. Electron transmission images were obtained using a Philips C20 TEM instrument. The tensile tests were performed at room temperature using a Thumler GmbH Tensile Tester Model equipped with a PA 6110 Nordic Transducer load cell with a maximum force of 250*N*. A crosshead speed of 10 mm min^{-1} was used for all samples. The width and the length of the specimens used for mechanical measurements were 3 cm and 12 cm respectively, while the effective length (the distance between the grips) was 6 cm. Prior any measurement, the samples were pre-equilibrated at 45 and 70% relative humidity. A Modulated DSC Model 2920 Thermal Advantage Instruments was used to measure the thermal properties of the films. Melting temperature (T_m) and heat of fusion (ΔH_m) were determined from the maximum position and the area of the melting peak respectively, by heating the samples from 25°C up to 250°C, with a rate of 5°C min^{-1}, using aluminum crucibles. Only the first heating was measured, due to film decomposition at around 225–250°C. The sorption isotherms were carried out on a gravimetric system consisting of a homemade stainless steel section for water vapor inlet and a CI Electronics Ltd® microbalance, equipped with metal vacuum enclosure (with a sensitivity of 0.1 μg) and Disbal® control unit. The mass changes, the vapor pressure and the cell temperature were continuously recorded by means of LabVIEW® software. The water permeability experiments were performed on a prototype stainless steel apparatus, equipped with Bronkhorst® mass and liquid flow controllers along with a control evaporator mixer (CEM) and Systech® moisture analyzers (Series 500). In the case of oxygen permeability a PBI Dansensor OPT-5000 instrument with a Thermo Fisher DC-10 temperature regulator was used, in compliance to ASTM F2622-08.[25] The permeability values presented in the manuscript were the average values of three permeation experiments. In all measurements the error was below 2%. All samples, prior to their testing, were conditioned in oven at a temperature of 50 ± 2°C for 48 h (ASTM

D 618 - Procedure B). Thermogravimetric analysis was performed on a SETARAM SETSYS Evolution 18 Analyzer, in the range of RT - 800°C, with a heating rate 5 K min^{-1} in a platinum crucible. A blank experiment was carried out in the same conditions and all the results are given after correction. The elemental composition for bentonite was determined through EDXRF measurements using a Philips PW2400 X-ray spectrometer.

Purification of bentonite

The purity (in montmorillonite) of raw bentonite clay used in this study was about 76%. The chemical composition (in wt %) was the following: SiO_2: 56.28, Al_2O_3: 14.66, TiO_2: 0.87, Fe_2O_3: 5.03, MgO: 4.2, CaO: 5.74, Na_2O: 2.39, K_2O:1.07, while the loss on ignition was 9.74%. The purification of raw clay was made through centrifugation, as follows: A 40 wt % raw bentonite solution in RO water was centrifuged three times at 4000 rpm for half an hour each time, and every time the upper part was kept. After the purification the Cation Exchange Capacity (CEC) increased to 88 meq/100 g (from initial 80) and the montmorillonite content ranged 90–92%, while impurities, such as quartz ($\sim$ 4%) and feldspar ($\sim$ 3%), still remained.[26] The produced suspension was found to have 1.52 wt % clay concentration and was used without any other treatment for the preparation of the nanocomposite films.

Preparation of the films

A 10 wt % PVA solution in water was produced by stirring for 6 h at 90°C and used as the basis for all the samples preparation. The samples were prepared by mixing the bentonite suspension with the polymer solution in quantities that gave 5, 10, and 20 wt % clay loading content on the produced films namely N05, N10, and N20, respectively. The mixture (100 mL) was stirred for half hour at 80°C and then sonicated for an extra half hour. The suspension (10–20 mL in regard to the final film thickness) was poured in square (12 $\times$ 12 cm) polystyrene Petri dishes and left to dry slowly at 25°C for 15 days. The average thickness of the samples used for permeability and mechanical tests was 0.1 $\pm$ 0.02 mm, while the average samples' thickness used for optical measurements was 50 $\pm$ 0.02 μm.

RESULTS AND DISCUSSION

Film morphology

Atomic force microscopy (AFM) has also become an important technique for the characterization of nanoparticles. Unlike TEM, AFM can provide size characterization in all three spatial dimensions, because it provides direct information about the height, as well as lateral dimensions of nanoparticles on surfaces. AFM has been used to characterize various types of exfoliated clay platelets.[27,28] Figure 1(a) shows the clay particles. It is clearly shown that the clay platelets have an average width of 70–150 nm. These values are in agreement with the values, obtained from literature in which, the layer of silicate clay mineral is about 1nm in thickness with platelets of around 100–200 nm in width.[29,30] Figure 1(b) shows the corresponding AFM image of N20 sample. A structure of the clay particles oriented on the surface of the sample is evident. The particles size about 70 nm account for the clay layers, which are oriented in plane with the sample's surface, while the lines observed in the figure having an approximate width of 20 nm, could be attributed to polymer chains, organized, due to space confinement. The same results are also obtained from TEM. The acquired images [Fig. 1(c,d)] revealed well dispersion of the clay particles into the polymer matrix in addition with well organized intercalated regions. Thus, the microscopic techniques (AFM and TEM), which in this study are used complementary to macroscopic ones, provide useful information about the nanocomposite morphology.

XRD measurements

Figure 2 shows the wide-angle X-ray diffraction patterns of pure PVA film, bentonite powder, and nanocomposite films prepared in this study. For the neat polymer a peak at $2\theta = 19.4^\circ$ can be attributed to PVA $10\bar{1}$ and 101 crystal reflections, corresponding to a *d* spacing of 4.57 Å.[31] Concerning the purified bentonite used in this study, the peak at $2\theta = 7^\circ$ corresponds to the 12.63 Å basal spacing, 001 reflection of the montmorillonite, while the peak around $2\theta = 28.6^\circ$ assigned to the impurities be presented in clay (mostly quartz and feldspar). For the N20 sample a peak was appeared at $2\theta = 3.2^\circ$, corresponding to a basal spacing of around 27 Å. This increase in basal spacing is due to the polymer intercalation in the clay galleries. These observations are in agreement with the results obtained from microscopic techniques. It must be noted that intercalated regions are obtained at lower clay concentrations than previous studies have reported.[14] This effect can be attributed to the presence of metal cations in the structure of the clay, which boost the polymer–clay interactions.

Conversely, a small shoulder corresponding to the characteristic peak of the clay basal spacing ($2\theta = 7^\circ$) is also present in XRD patterns. This indicates that a small part of the clay formed aggregates

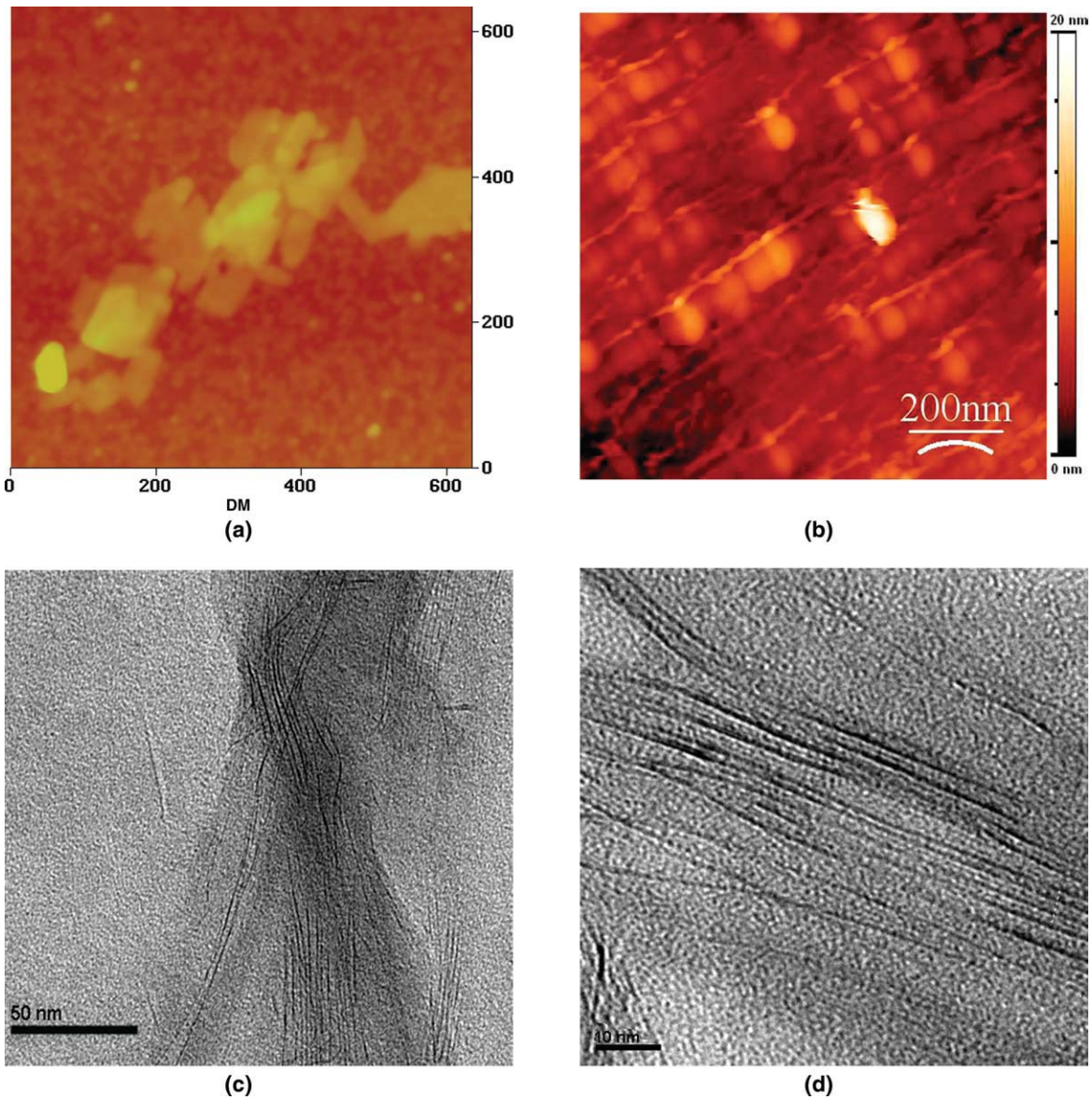

Figure 1 AFM images of (a) bentonite clay and (b) composite N20 film respectively, (c), (d) TEM images of N20. [Color figure can be viewed in the online issue, which is available at wileyonlinelibrary.com.]

during film formation. For the samples N05 and N10 the XRD patterns indicate a very good dispersion of the clay in the polymer matrix, since there is no significant peak evident around the expected 2θ angle (3–14°). In addition the increased background suggesting the existence of exfoliated inorganic layers throughout the polymer matrix.[14] The obtained results imply that the greatest quantity of the clay was exfoliated, while only a small amount of clay platelets was still remained as aggregates.

To investigate the orientation of clay nanoplatelets in the N20 sample, the film was fragmented into powder. The diffraction patterns of N20 sample in powder and film form (Fig. 3), revealed that the 001 peak of the clay is much more pronounced in the case of the film, giving evidence of well orientation of clay particles, parallel to the surface of the nanocomposite film. This result is also in agreement with preliminary neutron diffraction patterns obtained from lamellar and in-plane sample positions.[32]

UV-Vis spectroscopy

It is generally accepted that the optical clarity of the nanocomposites can be related to the dispersion of the inorganic particles into polymer matrix: well dispersion in nanoscale will lead to exfoliated composites high optical clarity.[33,34] On the other hand, clay aggregates, due to their sizes (200–700 nm), will lead to strong scattering and/or absorption, resulting in very low transmission of the UV light. Figure 4 shows the UV-Vis transmission spectra of the

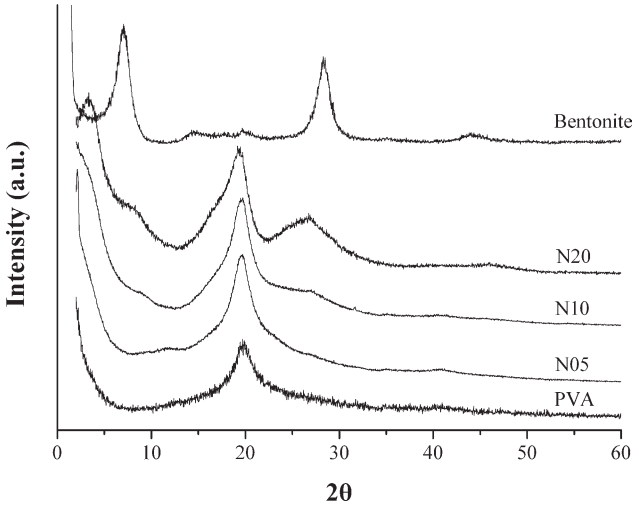

Figure 2 XRD patterns of pure PVA film, bentonite and nanocomposite films.

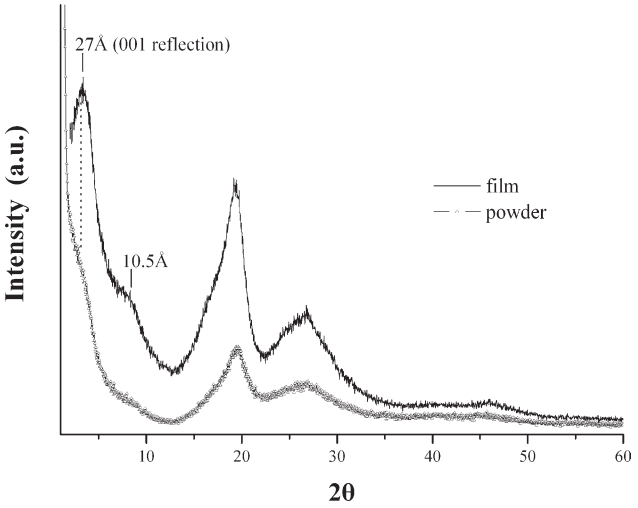

Figure 3 XRD patterns of N20 in film and powder form.

nanocomposites samples. The measured films had an average thickness of 50 μm. The nanocomposites samples retain the poly(vinyl alcohol)'s high optical clarity (above 95% in comparison with the pure PVA film) for the visible region (400–700 nm), due to well nanoscale dispersion of clay particles into the polymer matrix. It is also important to note that the samples have high optical clarity even in high clay loadings (10 and 20 wt %) contrary to other studies,[15] which reported that the clarity of a 20 wt % clay loading sample was decreased up to 26.5%. Thus, the high optical clarity in UV-Vis region of the nanocomposite samples prepared in this study can be attributed to the absence of clay aggregates in the region of 300–700 nm.

In the ultraviolet region, strong scattering/or absorption is observed, resulting in very low transmission of the UV light. This is not surprising as the typical particle sizes are 70–1000 nm. In the limiting case of 20% loading, there is an almost complete absorption of UV light below 300 nm, indicating that the N20 sample can potentially be used as a UV cut off filter.

Permeability of nanocomposites

The mass transport through a polymeric material is determined by the potential capacity of the polymer matrix to adsorb the penetrating molecules and by the ability of those molecules to diffuse through the polymeric material. The whole process can be described by two coefficients, namely:

- Solubility (S) - the partition coefficient of sorbed in regard to total molecules,
- Diffusivity (D) - the rate of transport of molecules through the polymeric matrix. The molecules' rate of transport through a polymer, as a result of the combined effects of diffusion and solubility, can be expressed by permeability coefficient (P_e), which is related to D and S by the expression[35]:

$$P_e = D \times S, \tag{1}$$

In this case, P_e incorporates both kinetic and thermodynamic properties of the polymer-permeant system.

On the other hand, the mass transport mechanism in the case of a nanoscale reinforced polymer is similar to that in a semicrystalline polymer: the transport mechanism within the polymeric matrix follows the Fick's law while the platelets act as impermeable barriers. Therefore, for polymer–clay nanocomposites, a

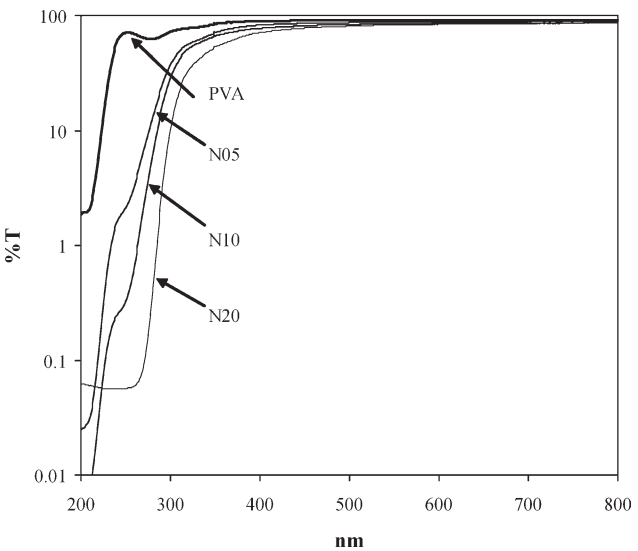

Figure 4 UV-Vis spectra of nanocomposites films.

TABLE I
Oxygen Permeability at Different Water Activities at 23°C

	Relative humidity			
Sample	0.50	0.65	0.75	0.85
	O_2 Permeability (ml cm/m^2.day)			
PVA	0.0023	0.035	0.215	1.88
N05	0.0012	0.028	0.200	1.71
N10	0.0008	0.023	0.185	1.58
N20	0.0003	0.019	0.148	1.54

decrease in solubility, due to reduced polymer volume, as well as in diffusion, due to more tortuous path, is expected. In general, three main factors are affecting the permeability in a nanocomposite: The volume fraction of the clay, their orientation relative to the diffusion direction and the aspect ratio of the platelets. Several models have been developed to predict the mass transfer within the nanocomposites. A simple permeability model for a regular arrangement of platelets has been proposed by Nielsen[36]:

$$\frac{P_e^{\text{comp}}}{P_e^{\text{matrix}}} = \frac{1-\varphi}{1+a/2\varphi}, \quad (2)$$

where P_e^{comp} and P_e^{matrix}, are the permeability coefficients for the composite and pure polymeric film respectively, $a = L/W$, is the aspect ratio of the nanoplatelets and φ, the volume fraction of the clay into the composite. The equation is valid up to volume fraction 10–15%, since at higher concentrations, the clay particles have a tendency to aggregate. Although its simplicity, Nielsen model has been widely accepted and fits the experimental observations well in several cases, especially for small volume fractions (below 10%).[37–39]

The results of oxygen permeability experiments, which were perform on samples having an area of 42 cm^2 and average thickness of around 100 μm, are summarized in Table I. It is clear that the permeability decreases as the volume fraction of clay in the composites increases, indicating that the clay particles are well dispersed and oriented in the polymeric matrix.

In Figure 5 it is shown the experimental permeability values at 23°C (square points) at different %RH, as a function of the clay volume fraction, φ, using $d_{\text{clay}} = 2.6$ g/cm^3 and $d_{\text{PVA}} = 1.3$ g/cm^3. The lines in the corresponding figure present the theoretical values obtained by Nielsen model using the aspect ratio values that provide the best fitting to the experimental results. In the case of 50% RH, a value of $L/W = 70$ is derived. This value, which is in agreement with both the theoretical one for the aspect ratio of bentonite platelets and the experimental one obtained from AFM technique, implies that the greatest portion of the clay is delaminated within the polymer matrix,[40] while a small amount may also form aggregates. This conclusion is in agreement with the results obtained from the macroscopic and the XRD techniques.

In addition, oxygen permeability measurements at higher relative humidity (%RH)—relative oxygen permeability experiments—exhibit a significant increase in permeability, although the values of nanocomposite films are much lower than the corresponding of the pure PVA. As relative humidity increases, the aspect ratio values predicted by the Nielsen model, gradually decreases—from 70 at 50% RH to 2 at 85% RH. This behavior can be attributed to the fact that water acts as plasticizer, increasing the polymer free volume and reducing the crystallinity of the polymer. The free volume's increase facilitates the diffusion process because of the creation of easier pathways for the solutes. In addition the crystallites are considered to be impermeable to the gas molecules. Both effects facilitate the transport of oxygen molecules leading to an increase in permeability. Thus, the barrier effect of clays becomes less significant, reflecting a decrease in the aspect ratio values estimated by Nielsen model.

Furthermore, the well dispersion of inorganic particles into the polymer matrix leads to a significant decrease in water permeability as the clay content increases. Again, the reduced permeability of nanocomposites at certain relative humidity should mainly be attributed to the increase in tortuosity caused by the impermeable platelets while there is also a reduction in solubility similar to semicrystalline polymers. On the other hand, a significant increase in permeability as a function of %RH is

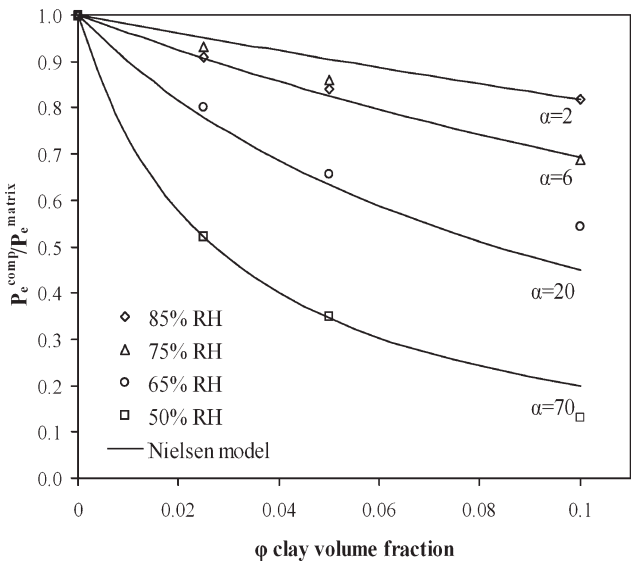

Figure 5 Oxygen permeability ratio of composite films in relation to pure polymer film (points) at different %RH and predictions based on Nielsen model.

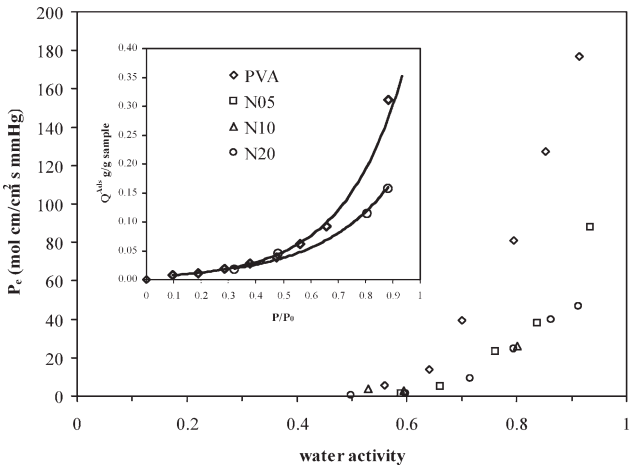

Figure 6 Water permeability as a function of water activity. Insert: water sorption isotherms.

observed for all samples. This trend can be explained in terms of solubility and diffusivity coefficients. The solubility of water in polymers can be described either by Henry's law or by Flory-Huggins theory. Because of its highly polar nature, two kinds of phenomena coexist depending on the nature of the polymer: (a) Diffusion coefficient (D) of water in hydrophilic polymers generally increases as concentration of water also increases and (b) Solubility increases exponentially with vapor pressure. Consequently permeation rate increases non linearly with vapor pressure difference and also becomes dependent on absolute vapor pressure. Therefore, the permeability versus water activity curves exhibit a great enhancement at high %RH, similar to the trend of water isotherm (Fig. 6).

Generally, in nanocomposites, the presence of inorganic phase can influence the size and the number of the free volume holes, especially at the interfaces. Consequently, the change in the permeability of such systems is a balance between the barrier properties of the impermeable nanoplatelets and the possible increase of the free volume of the matrix.[41] It has been noticed that the interaction between certain polymer matrices and nanoplatelets can affect crystallinity, molecular orientation, and packing of the molecules near the nanoplatelets.[41] The alteration of the molecular packing around the nanoplatelets may further enhance the barrier properties of polymer nanocomposites. On the other hand, poor interface interactions between nanoplatelets and matrix will usually result in decreased barrier properties.[42–44]

Thermogravimetric analysis

Figure 7 shows the TGA curves of the PVA/bentonite clay nanocomposites under N_2 flow (30 mL/min). It is notable that the clay acts protectively against the polymer thermal degradation, at temperatures above 400°C, where the polymer retains almost 50% of its initial mass. This enhancement in the thermal stability is due to the presence of clay nanolayers, which can act as barriers maximizing the heat insulation and minimizing the permeability of volatile degradation products to the material.

Differential scanning calorimetry measurements

The thermal behavior of the samples was also tested using Differential Scanning Calorimetry. For the nanocomposites, no thermal transitions were observed between 50 and 170°C. The absence of thermal events, in this region, is in agreement with the general behavior of polymers intercalated in clays.[45] At higher temperatures, two distinct and overlapping melting peaks were detected: one around the bulk T_m and another one at higher melting temperature (about 10–15°C) [Fig. 8(a)]. The second peak in DSC curves can be attributed to the existence of new polymer crystalline phase, induced by the presence of the clays. These findings are in agreement with the results obtained from the study of similar polymer–clay systems.[14]

To quantify the relative volumes of the two phases present, we fitted the DSC data with Gaussian functions, to estimate the melting enthalpies at different clay content. Thus, a plot of the fraction of the two melting enthalpies versus clay loading was drawn [Fig. 8(b)]. It seems that the new crystalline form, increases linearly with the amount of clays in the polymeric matrix and at the expense of the bulk-like PVA crystal phase, revealing that the new high-T_m phase is induced by the presence of the bentonite layers (Table II). In addition, the linear increase in the enthalpy of this phase with the clay content,

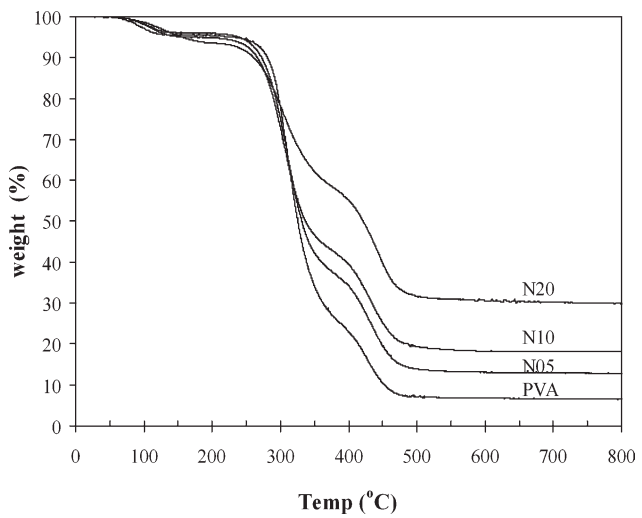

Figure 7 Thermogravimetric analysis of pure PVA and produced nanocomposites films.

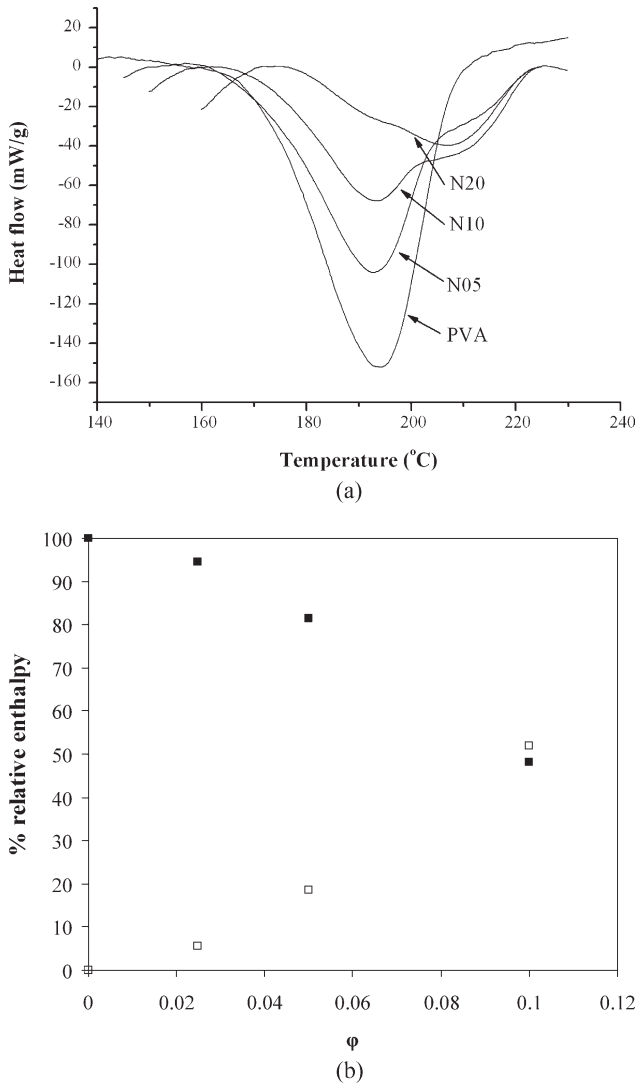

Figure 8 (a) DSC curves in the melting region. (b) Fraction of the heats of fusion for the two phases (closed symbols: bulklike phase, open symbols: clay induced phase).

suggests that the inorganic layers are well dispersed, either intercalated or exfoliated, in the polymer. The calculated clay content, at which the enthalpies of the two phases are equal, is much lower than the values demonstrated in previous studies,[14] revealing that in this case the polymer–clay interactions are more effective. On the other hand, the PVA enthalpy decreases with the clay content, since the clay particles prohibit polymer crystals formation by occupying hydroxyl groups of the PVA.

TABLE II
Differential Scanning Calorimetry Results

Sample	T_1 °C	Enthalpy$_1$ J/g	T_2 °C	Enthalpy$_2$ J/g	X_c*%
PVA	191.6	40.0	–	–	29
N05	191.3	32.1	214.1	1.5	23
N10	193.0	22.0	211.8	4.5	16
N20	194.8	7.5	209.2	6.5	5

* The crystallinity fraction of the samples was determined from the first peak's melting enthalpy (Enthalpy for 100% crystalline PVA 138 J/g). The indexes 1 and 2 refer to the PVA and clay induced melting peaks accordingly.

Mechanical properties

Table III summarizes the results on the mechanical properties of the samples. The experiments were performed at ambient humidity (~ 50%) while the samples were pre-equilibrated at 45 and 70% RH prior measurement. For 45% RH the Young's modulus of the samples increased with increasing clay content and it was around 60% more on 5 wt % clay addition and 260% more with 20 wt %. The ultimate tensile strength of the samples was less influenced by the clay content, reaching a maximum increase of 60% for the N20 sample. On the other hand, at 70%RH, the Young's modulus was greatly affected by clay content. Thus, for the N05 sample, the increase was more than nine times and for N20 almost 193 times, respectively. This behavior can be attributed to the fact that, while PVA losses great percentage of its mechanical properties, clay's strength remains unaffected by water. The ultimate tensile strength was increased in a much larger extend in regard to the 45% RH samples. For the N20 sample the corresponding increase was more than 3.5 times. The main reason for the drastic improvement in tensile modulus in PVA nanocomposites is the strong interaction between matrix and

TABLE III
Mechanical Properties of the Samples

	Relative humidity					
	0.45			0.7		
Sample	Elongation (%)	Ultimate Tensile Strength (MPa)	Young's Modulus (GPa)	Elongation (%)	Ultimate Tensile Strength (MPa)	Young's Modulus (GPa)
PVA	99 ± 11.2	40 ± 0.8	1.25 ± 0.3	250 ± 21.0	14 ± 1.4	0.011 ± 0.002
N05	54 ± 4.6	39 ± 1.1	2.00 ± 0.5	220 ± 18.2	22 ± 1.3	0.104 ± 0.04
N10	18 ± 2.1	42 ± 1.3	2.18 ± 0.2	170 ± 15.5	28 ± 2.6	0.25 ± 0.08
N20	9 ± 1.2	62 ± 0.9	3.25 ± 0.3	20 ± 1.6	51 ± 1.5	2.17 ± 0.5

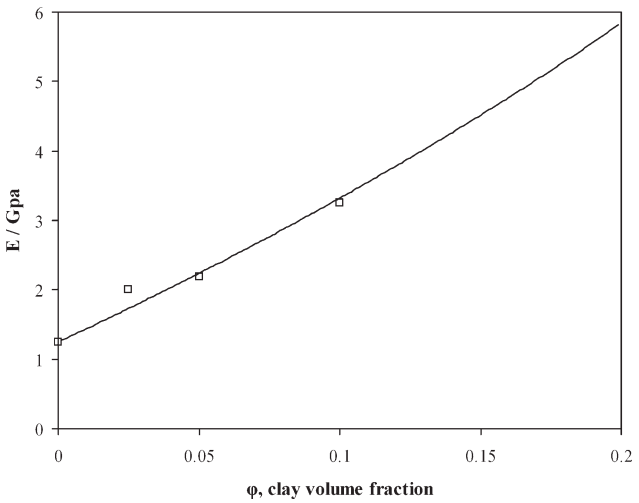

Figure 9 Young's modulus (points) for 45% RH and Halpin - Tsai prediction (line) for aspect ratio $\alpha = 8$.

silicate layers via formation of hydrogen bonds due to the strong hydrophilicity of the clay edges.[46,47]

The Young's modulus data of the nanocomposites can be fit to models in order to estimate the aspect ratios of the reinforced particles.[48] These models include the equation proposed by Halpin-Tsai[49,50]:

$$\frac{E}{E_0} = \frac{1 + 2a\eta\varphi}{1 - \eta\varphi}, \tag{3}$$

where E and E_0, are the Young's moduli of the nanocomposites and pure polymer respectively, α, is the aspect ratio of the particles, φ, is the volume fraction of the fillers and η, is a coefficient given by the following equation:

$$n = \left[\frac{(E_f/E_0) - 1}{(E_f - E_0) + 2a}\right], \tag{4}$$

where E_f is the Young's modulus of the clay platelets, which was taken as 170 GPa.[51] Concerning the mechanical properties, Halpin-Tsai equation is one of the most versatile and widely used semiempirical equations for the polymeric composites and blends.[52,53]

Figure 9 presents the experimental data and the prediction using the abovementioned model, with clay particle aspect ratio equal to 8. At higher relative humidity, due to the samples' different degree of swelling, the model can not be effectively applied.

It must be noted, that the aspect ratio calculated from permeability data (Nielsen equation) should be in agreement with the value obtained from the mechanical strength measurements, using Halpin-Tsai model. This is not the case in our samples, since the estimated values differ almost one order of magnitude. The incongruity observed may be attributed to the specific orientation of the clay particles parallel to the film surface. Consequently, the intercalated inorganic layers, being perpendicular assembled to the direction of flow path, affect significant the permeability properties of the composites. On contrary, their influence, in the case of in plane mechanical measurements, becomes less important.

CONCLUSIONS

A series of nanocomposite materials that consist of PVA and bentonite clay were prepared by effectively dispersing the inorganic nanolayers into PVA matrix, via solvent casting technique. The produced materials were studied by microscopic and macroscopic techniques. Morphological studies using AFM and TEM, revealed the excellent dispersion of the clay particles into the polymer matrix in addition with well organized intercalated regions. These results are in agreement with the obtained XRD patterns, in which the 001 peak of the clay is much more pronounced in the case of film, than in powder form.

Thermal stability, mechanical strength and optical clarity of PVA/clay composites were also investigated by TGA, DSC, and UV-visible transmission spectra, respectively. The effective incorporation of clay nanolayers within the polymer matrix leaded to an increase in thermal decomposition temperature and to enhanced mechanical properties. Furthermore, DSC curves demonstrated the existence of new polymer crystalline phase, induced by the presence of the clays. This attribute has also been observed in similar studies. Furthermore, the UV-visible transmission spectra exhibited that, contrary to other studies, the samples retained high optical clarity, even at high clay loadings (20 wt %).

In addition, water and oxygen permeability measurements, revealed the improved barrier properties of the developed composites. The experimental data are in good agreement with the theoretical models, predicting the permeability coefficients in composite systems.

The final properties of a composite are determined by the competitive effects of polymer–polymer and polymer–clay interactions. In our case, the presence of the acetoxy groups in the PVA, leads to weaker intrapolymer interactions together with increased interfacial bonding with the clay. Both effects enable the formation of organized polymer/clay assemblies, enhancing the overall material's performance.

References

1. Giannelis, E. M. Appl Organometal Chem 1998, 12, 675.
2. Ogawa, M.; Kuroda, K. Bull Chem Soc Jpn 1997, 70, 2593.
3. Alexandre, M.; Dubois, P. Mater Sci Eng 2000, 28, 1.

4. Kojima, Y.; Usuki, A.; Kawasumi, M.; Okada, A.; Fukushima, Y.; Karauchi, T.; Kamigaito, O. J Mater Res 1993, 6, 1185.
5. Lan, T.; Kaviratna, P. D.; Pinnavaia, T. J. Chem Mater 1994, 6, 573.
6. Wang, Z.; Pinnavaia, T. J. Chem Mater 1998, 10, 3769.
7. Yeh, J.-M.; Liou, S.-J.; Lai, C.-Y.; Wu, P.-C.; Tsai, T.-Y. Chem Mater 2001, 13, 1131.
8. Jiankun, L.; Yucai, K.; Zongneng, Q.; Xiao-Su, Y. J Polym Sci Part B: Polym Phys 2001, 39, 115.
9. Podsiadlo, P.; Kaushik, A. K.; Arruda, E. M.; Waas, A. M.; Shim, B. S.; Xu, J.; Nandivada, H.; Pumplin, B. G.; Lahann, J.; Ramamoorthy, A.; Kotov, N. A. Science 2007, 318, 80.
10. Gilman, J. W.; Jackson, C. L.; Morgan, A. B.; Harris, R.; Manias, E.; Giannelis, E. P.; Wuthenow, M.; Hilton, D.; Philips, S. H. Chem Mater 2000, 12, 1866.
11. Fischer, H. Mater Sci Eng C 2003, 23, 763.
12. Giannelis, E. P. Adv Mater 1996, 8, 29.
13. Carrado, A. K.; Thiyagarajan, P.; Elder, L. D. Clay Clay Miner 1996, 44, 506.
14. Strawhecker, K. E.; Manias, E. Chem Mater 2000, 12, 2943.
15. Yu, Y. H.; Lin, C. Y.; Yeh, J. M.; Lin, W. H. Polymer 2003, 44, 3553.
16. Grunlan, J. C.; Grirorian, A.; Hamilton, C. B.; Mehrabi, A. R. J Appl Polym Sci 2004, 93, 1102.
17. Chang, J. H.; Jang, T. G.; Ihn, K. J.; Lee, W. K.; Sur, G. S. J Appl Polym Sci 2003, 90, 3208.
18. Kokabi, M.; Sirousazar, M.; Hassan, Z. M. Eur Polym Mater 2007, 43, 773.
19. Adoor, S. G.; Sairam, M.; Manjeshwar, R. K. V. S. N.; Aminabhavi, T. M. J Mem Sci 2006, 285, 182.
20. Ikhsan, J.; Wells, J. D.; Johnson, B. B.; Angove, M. J. Colloid Surf A 2005, 252, 33.
21. Stathi, P.; Papadas, I. T.; Enotiadis, A.; Gengler, R. Y. N.; Gournis, D.; Rudolf, P.; Deligiannakis, Y. Langmuir 2009, 25, 6825.
22. Mortland, M. M.; Raman, K. V. Clays Clay Miner 1968, 16, 393.
23. Lim, Y. T.; Park, O. O. Rheol Acta 2001, 40, 220.
24. Lee, S. S.; Hur, M. H.; Yang, H.; Lim, S.; Kim, J. J Appl Polym Sci 2006, 101, 2749.
25. ASTM F2622-08 - Standard Test Method for Oxygen Gas Transmission Rate Through Plastic Film and Sheeting Using Various Sensors. Available at: http://www.astm.org/Standards/F2622.htm.
26. Christidis, G. E.; Scott, P. W.; Marcopoulos, T. Clay Clay Miner 1995, 43, 6377.
27. Piner, R. D.; Xu, T. T.; Fisher, F. T.; Qiao, Y.; Ruoff, R. S. Langmuir 2003, 19, 7995.
28. Ploehn, H. J.; Liu, C. Ind Eng Chem Res 2006, 45, 7025.
29. Hussain, F.; Hojjati, M.; Okamoto, M.; Gorga, R. E. J Comp Mater 2006, 40, 1511.
30. Usuki, A.; Hasegawa, N.; Kato, M. Adv Polym Sci 2005, 179, 135.
31. Assendert, H. E.; Windle, A. H. Polymer 1998, 39, 4295.
32. Katsaros, F. K.; Steriotis, Ô. A.; Sapalidis, A. A.; Favvas, E. P. In Neutron Diffraction Studies of Polymer/Clay Nanocomposites. BENSC Experimental Reports 2008; Rodig, A.; Brandt, A.; Graf, H. A., Eds.; Helmholtz-Zentrum Berlin für Materialien und Energie GmbH; Berlin, 2009, p 212.
33. Gusev, A. A.; Lusti, H. R. Adv Mater 2001, 13, 1641.
34. Schmidt, G.; Malwitz, M. M. Curr Opin Colloid Interf Sci 2003, 8, 103.
35. Crank, J. The Mathematics of Diffusion, 2nd ed., Clarendon: Oxford, 1975, p 46.
36. Nielsen, L. E. J Macromol Sci Chem A 1967, 1, 929.
37. Sun, L.; Boo, W.-J.; Clearfield, A.; Sue, H.-J.; Pham, H. Q. J Membr Sci 2008, 318, 129.
38. Lan, T.; Kaviratna, P. D.; Pinnavaia, T. J. Chem Mater 1994, 6, 573.
39. Wang, Y.; Zhang, H.; Wu, Y.; Yang, J.; Zhang, L. Eur Polym Mater 2005, 41, 2776.
40. Ray, S. S.; Bousmina, M. Prog Mater Sci 2005, 50, 962.
41. Incarnato, L.; Scarfato, P.; Russo, G. M.; Di Maio, L.; Iannelli, P.; Acierno, D. Polymer 2003, 44, 4625.
42. Chaiko, D. J.; Leyva, A. A. Chem Mater 2005, 17, 13.
43. Osman, M. A.; Mittal, V.; Morbidelli, M.; Suter, U. W. Macromolecules 2003, 36, 9851.
44. Osman, M. A.; Mittal, V.; Morbidelli, M.; Suter, U. W. Macromolecules 2004, 37, 7250.
45. Anastasiadis, S. H.; Karatasos, K.; Vlachos, G.; Giannelis, E. P.; Manias, E. Phys Rev Lett 2000, 84, 915.
46. Sengwa, R. J.; Choudhary, S.; Sankhla, S. Colloid Surf A: Phys Eng Aspect 2009, 336, 79.
47. Jung, H. M.; Lee, E. M.; Ji, B. C.; Deng, Y.; Yun, J. D.; Yeum, J. H. Colloid Polym Sci 2007, 285, 705.
48. Nielsen, L. E.; Landel, R. F.; Mechanical Properties of Polymers and Composites; Marcel Dekker: New York, 1994.
49. Halpin, J. C. Effects of environmental factors on composite materials. AFML-TR-67–423, 1969.
50. Halpin, J. C.; Kardos, J. L. Polym Eng Sci 1976, 16, 344.
51. Shia, D.; Hui, C. Y.; Burnside, S. D.; Giannelis, E. P. Polym Compos 1998, 19, 608.
52. Derakhshandeh, B.; Shojaei, A.; Faghihi, M. J Appl Polym Sci 2008, 108, 3808.
53. Tarapow, J. A.; Bernal, C. R.; Alvarez, V. A. J Appl Polym Sci 2009, 111, 768.